Inorganic Chemistry

Article

pubs.acs.org/IC

Ultralarge 3d/4f Coordination Wheels: From Carboxylate/Amino Alcohol-Supported $\{Fe_4Ln_2\}$ to $\{Fe_{18}Ln_6\}$ Rings

Olga Botezat,[†,‡] Jan van Leusen,[‡] Victor Ch. Kravtsov,[†] Paul Kögerler,*[,‡] and Svetlana G. Baca*[,†]

[†]Institute of Applied Physics, Academy of Sciences of Moldova, 2028 Chisinau, Moldova

[‡]Institute of Inorganic Chemistry, RWTH Aachen University, 52074 Aachen, Germany

Supporting Information

ABSTRACT: A family of wheel-shaped charge-neutral heterometallic $\{Fe^{III}_4Ln^{III}_2\}$- and $\{Fe^{III}_{18}M^{III}_6\}$-type coordination clusters demonstrates the intricate interplay of solvent effects and structure-directing roles of semiflexible bridging ligands. The $\{Fe_4Ln_2\}$-type compounds $[Fe_4Ln_2(O_2CCMe_3)_6(N_3)_4(Htea)_4]\cdot 2(EtOH)$, Ln = Dy (**1a**), Er (**1b**), Ho (**1c**); $[Fe_4Tb_2(O_2CCMe_3)_6(N_3)_4(Htea)_4]$ (**1d**); $[Fe_4Ln_2(O_2CCMe_3)_6(N_3)_4(Htea)_4]\cdot 2(CH_2Cl_2)$, Ln = Dy (**2a**), Er (**2b**); $[Fe_4Ln_2(O_2CCMe_3)_4(N_3)_6(Htea)_4]\cdot 2(EtOH)\cdot 2(CH_2Cl_2)$, Ln = Dy (**3a**), Er (**3b**) and the $\{Fe_{18}M_6\}$-type compounds $[Fe_{18}M_6(O_2CCHMe_2)_{12}(Htea)_{18}(tea)_6(N_3)_6]\cdot n(\text{solvent})$, M = Dy (**4**, **4a**), Gd (**5**), Tb (**6**), Ho (**7**), Sm (**8**), Eu (**9**), and Y (**10**) form in ca. 20−40% yields in direct reaction of trinuclear Fe^{III} pivalate or isobutyrate clusters, lanthanide/yttrium nitrates, and bridging triethanolamine (H_3tea) and azide ligands in different solvents: EtOH for the smaller $\{Fe_4Ln_2\}$ wheels and MeOH/MeCN or MeOH/EtOH for the larger $\{Fe_{18}M_6\}$ wheels. Single-crystal X-ray diffraction analyses revealed that **1**−**3** consist of planar centrosymmetric hexanuclear clusters built from Fe^{III} and Ln^{III} ions linked by an array of bridging carboxylate, azide, and aminopolyalcoholato-based ligands into a cyclic structure with a cavity, and with distinct sets of crystal solvents (2 EtOH per formula unit in **1a**−**c**, 2 CH_2Cl_2 in **2**, and 2 EtOH and 2 CH_2Cl_2 in **3**). In **4**−**10**, the largest 3d/4f wheels currently known, nearly linear Fe_3 fragments are joined via mononuclear Ln/Y units by a set of isobutyrates and amino alcohol ligands into virtually planar rings. The magnetic properties of **1**−**10** reveal slow magnetization relaxation for $\{Fe_4Tb_2\}$ (**1d**) and slow relaxation for $\{Fe_4Ho_2\}$ (**1c**), $\{Fe_{18}Dy_6\}$ (**4**), and $\{Fe_{18}Tb_6\}$ (**6**).

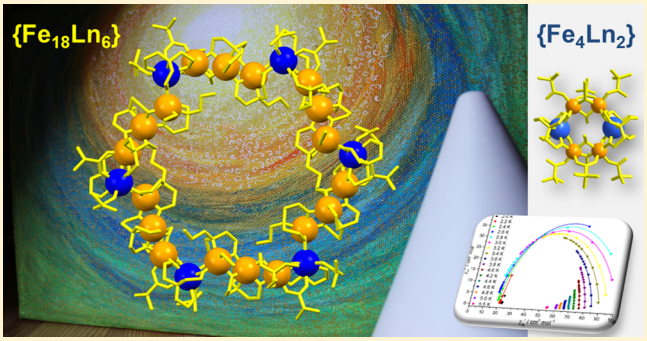

INTRODUCTION

Wheel-shaped high-nuclearity metal clusters of paramagnetic ions, which can be regarded as chains with a finite number of spin centers, have received substantial attention, largely stimulated by their fascinating physical properties, including single-molecule magnet (SMM) and spin qubit characteristics.[1] In this field pioneering synthesis efforts have mainly focused on the design and investigation of pure 3d systems: the "ferric wheels" reported by Lippard, Christou, and their cowokers[2] or by "manganese wheels" prepared by Christou et al.,[3] a "nickel wheel"[4] and a "chromium wheel"[5] reported by Winpenny and Timco et al., lately extended to fascinating heterometallic $\{Cr_7M\}$ and $\{Cr_8M\}$ wheels.[6] Increasing interest in the molecular magnetic anisotropy of such clusters led to the integration of lanthanide (4f) ions.[7] In 2010 the group of Murray[8] reported the first $\{Dy_6\}$ wheel that exhibits slow magnetization relaxation. This development has been followed by the construction of heterometallic d/f wheel-shaped clusters, that combine highly anisotropic Ln^{III} ions with the large spin values derived from exchange-coupled transition metal ions, but only very few d/f wheel-based SMMs have been discovered thus far.[9]

Of special interest in this context are wheel-shaped polynuclear Fe^{III}-Ln^{III} SMM clusters, and to our knowledge, only $\{Fe_4Dy_4\}$ and $\{Fe_4Ln_2\}$ (Ln^{III} = Eu, Lu) wheels were described in literature by Powell et al.[10] Moreover, the development of general synthetic routes toward novel heterometal coordination clusters with wheel topologies represent an ongoing challenge.

Among different strategies for the preparation of metallic wheels, the use of alkoxides as chelating and bridging ligands has been successful in many cases.[8,11] We also explored the potential of using both structure-directing amino alcohols and carboxylate bridges for the synthesis of heterometallic coordination cluster families.[12,13a] Using recent advances in synthetic methodology and expanding our development efforts for large polynuclear iron systems,[13] we herein report a straightforward protocol to heterometallic Fe/Ln (or Fe/Y) wheels using trinuclear μ-oxo Fe^{III} pivalate or isobutyrate precursors and tetratopic triethanolamine (H_3tea) and azide ligands, both capable to bridge different types of metal ions

Received: September 8, 2016
Published: January 30, 2017

DOI: 10.1021/acs.inorgchem.6b02100
Inorg. Chem. 2017, 56, 1814−1822

(Figure 1). This approach resulted in a remarkable family of hexanuclear $\{Fe_4Ln_2\}$-type wheel-shaped compounds, namely,

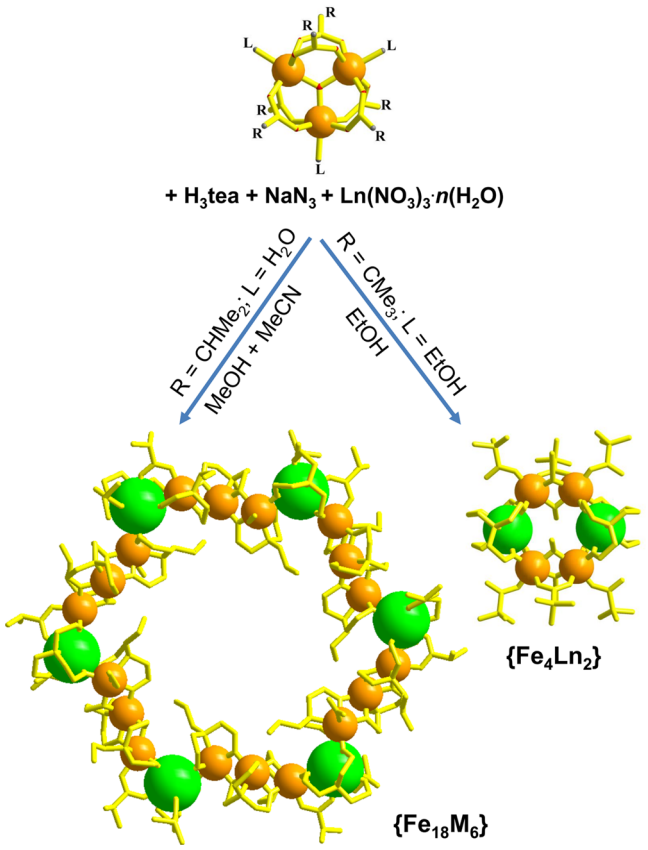

Figure 1. Schematic syntheses of $\{Fe_4Ln_2\}$-type (**1**) and $\{Fe_{18}M_6\}$-type (M = Ln: **4**–**9**; M = Y: **10**) compounds.

$[Fe_4Ln_2(O_2CCMe_3)_6(N_3)_4(Htea)_4]\cdot 2(EtOH)$, Ln^{III} = Dy (**1a**), Er (**1b**), Ho (**1c**), and $[Fe_4Tb_2(O_2CCMe_3)_6(N_3)_4(Htea)_4]$ (**1d**), $[Fe_4Ln_2(O_2CCMe_3)_6(N_3)_4(Htea)_4]\cdot 2(CH_2Cl_2)$, Ln^{III} = Dy (**2a**), Er (**2b**), and $[Fe_4Ln_2(O_2CCMe_3)_4(N_3)_6(Htea)_4]\cdot 2(EtOH)\cdot 2(CH_2Cl_2)$, Ln^{III} = Dy (**3a**), Er (**3b**), as well as in the currently largest (24-nuclear) 3d/4f wheels, $[Fe_{18}M_6(O_2CCHMe_2)_{12}(Htea)_{18}(tea)_6(N_3)_6]\cdot n(solvent)$, M^{III} = Dy (**4**, **4a**), Gd (**5**), Tb (**6**), Ho (**7**), Sm (**8**), Eu (**9**), and Y (**10**), where H_3tea = triethanolamine.

EXPERIMENTAL SECTION

Materials and Instrumentations. All reagents were purchased from commercial sources and used without further purification. All synthetic procedures have been performed under aerobic conditions using commercial-grade solvents. $[Fe_3O(O_2CCMe_3)_6(H_2O)_3]\cdot O_2CCMe_3\cdot 2(Me_3CCO_2H)$, $[Fe_3O(O_2CCMe_3)_6(EtOH)_3]NO_3\cdot(EtOH)$, $[Fe_6O_2(OH)_2(O_2CCMe_3)_{12}]$, and $[Fe_3O(O_2CCHMe_2)_6(H_2O)_3]NO_3\cdot 2(MeCN)\cdot 2(H_2O)$ were prepared by using method described in the literature.[13a,b] A Bandelin Sonorex RK-100H ultrasonic bath operating at 35 kHz with a maximum power output of 160 W was used for ultrasonic irradiation in the syntheses of **4**–**10**.

IR spectra (4000–400 cm^{-1}) were recorded on a PerkinElmer Spectrum One spectrometer using KBr pellets. Thermogravimetric analysis/differential thermal analysis (TGA/DTA) measurements were performed with a Mettler Toledo TGA/SDTA 851 in dry N_2 (60 mL min^{-1}) at a heating rate of 10 K min^{-1} from 25 to 800 °C for **1**–**3** (Figures S24–S30) and at a heating rate of 5 K min^{-1} from 25 to 1000 °C for **4**–**10** (Figures S31–S38). Metal analysis was performed using inductively coupled plasma-optical emission spectroscopy (ICP-OES) at ZEA-3, Research Centre Jülich.

*Syntheses of $[Fe_4Ln_2(O_2CCMe_3)_6(N_3)_4(Htea)_4]\cdot 2(EtOH)$ (Ln^{III} = Dy (**1a**); Er (**1b**); Ho (**1c**)).* Compounds **1a**–**c** can be prepared by two methods starting from trinuclear (A) or hexanuclear (B) ferric pivalates:

Method A. A solution of $[Fe_3O(O_2CCMe_3)_6(EtOH)_3]NO_3\cdot(EtOH)$ (0.208 g, 0.2 mmol), $Ln(NO_3)_3\cdot xH_2O$ (0.3 mmol), NaN_3 (0.038 g, 0.6 mmol), and H_3tea (0.084 g, 0.6 mmol) in 10 mL of EtOH was heated under reflux (ca. 78 °C) for 30 min and then filtered. The filtrate was kept in a closed vial at room temperature. After two weeks, yellow crystals of **1a**–**c**, suitable for single-crystal X-ray analysis, were filtered off, washed with EtOH, water, and MeCN, and dried in air. Yield (based on Fe): 0.084 g, 28% (**1a**); 0.100 g, 33% (**1b**); 0.065 g, 22% (**1c**). After removal of **1** from the mixture, well-defined dark-brown crystals of $[Fe_8O_3(O_2CCMe_3)_6(N_3)_3(tea)(Htea)_3]\cdot 0.5(EtOH)$[13a] formed in ca. 30% yield if the filtrate was kept in a closed vial at room temperature for several additional weeks.

Method B. A solution of $[Fe_6O_2(OH)_2(O_2CCMe_3)_{12}]$ (0.161 g, 0.1 mmol), $Ln(NO_3)_3\cdot xH_2O$ (0.3 mmol), NaN_3 (0.038 g, 0.6 mmol), and H_3tea (0.084 g, 0.6 mmol) in 10 mL of EtOH was heated under reflux for 30 min and then filtered. The filtrate was stored in a closed vial at room temperature. After two weeks, the yellow crystals of **1a**–**c** suitable for a single-crystal X-ray diffraction analysis were filtered off, washed with EtOH, water, and MeCN, and dried in air. Yield (based on Fe): 0.075 g, 25% (**1a**); 0.130 g, 43% (**1b**); 0.060 g, 20% (**1c**). Dark brown crystals of $[Fe_8O_3(O_2CCMe_3)_6(N_3)_3(tea)(Htea)_3]\cdot 0.5(EtOH)$ also slowly formed in the mother liquor once the yellow crystals of **1** had been removed.

The identity of **1a**–**c** prepared by method B was established from their IR data, elemental and TG analyses, as well as by a single-crystal X-ray diffraction analysis.

1a *{Fe_4Dy_2}.* Elemental analysis calcd. for $C_{58}H_{118}Dy_2Fe_4N_{16}O_{26}$ (2004.1 g mol^{-1}): C 34.76, H 5.93, N 11.15%; found: C 33.61, H 5.68, N 10.46%; calcd. mass ratio of Dy/Fe: 1.45; found: 0.85. IR (KBr): ν = 3434 (br, m), 2958 (m), 2899 (m), 2865 (m), 2098 (s), 2076 (vs), 2058 (sh), 1582 (sh), 1536 (vs), 1481 (s), 1459 (m), 1420 (s), 1402 (s), 1353 (m), 1284 (m), 1226 (m), 1152 (w), 1098 (m), 1074 (m), 1024 (m), 918 (sh), 902 (m), 836 (w), 787 (w), 741 (w), 650 (m), 624 (m), 603 (m), 569 (m), 553 (sh), 489 (m), 428 (m) cm^{-1}.

1b *{Fe_4Er_2}.* Elemental analysis calcd. for $C_{58}H_{118}Er_2Fe_4N_{16}O_{26}$ (2011.6 g mol^{-1}): C 34.60, H 5.91, N 11.13%; found: C 32.72, H 5.92, N 11.20%; calcd. mass ratio of Er/Fe: 1.50; found: 1.50. IR (KBr): ν = 3422 (br, m), 2958 (m), 2900 (m), 2866 (m), 2099 (s), 2076 (vs), 2058 (sh), 1582 (sh), 1535 (vs), 1481 (s), 1459 (m), 1420 (s), 1403 (s), 1354 (m), 1284 (m), 1226 (m), 1153 (w), 1098 (m), 1075 (m), 1024 (m), 920 (sh), 902 (m), 836 (w), 787 (w), 742 (w), 655 (m), 626 (m), 602 (m), 568 (m), 555 (sh), 492 (m), 426 (m) cm^{-1}.

1c *{Fe_4Ho_2}.* Elemental analysis calcd. for $C_{58}H_{118}Fe_4Ho_2N_{16}O_{26}$ (2008.9 g mol^{-1}): C 34.68, H 5.92, N 11.16%; found: C 32.77, H 5.87, N 11.51%; calcd. mass ratio of Ho/Fe: 1.48; found: 1.52. IR (KBr): ν = 3440 (br, m), 2958 (m), 2899 (m), 2865 (m), 2099 (s), 2076 (vs), 2058 (sh), 1582 (sh), 1535 (vs), 1481 (s), 1459 (m), 1420 (s), 1402 (s), 1353 (m), 1284 (m), 1227 (m), 1152 (w), 1098 (m), 1074 (m), 1024 (m), 919 (sh), 902 (m), 787 (w), 742 (w), 653 (m), 625 (m), 602 (m), 567 (m), 554 (sh), 491 (m), 426 (m) cm^{-1}.

*Synthesis of $[Fe_4Tb_2(O_2CCMe_3)_6(N_3)_4(Htea)_4]$ (**1d**) {Fe_4Tb_2}.* A solution containing $[Fe_6O_2(OH)_2(O_2CCMe_3)_{12}]$ (0.161 g, 0.1 mmol), $Tb(NO_3)_3$ (0.103 g, 0.3 mmol), NaN_3 (0.038 g, 0.6 mmol), and H_3tea (0.084 g, 0.6 mmol) in 10 mL of EtOH was refluxed for 30 min and then filtered. The filtrate was stored in a closed vial at room temperature. After two months, red and yellow crystals formed and were filtered off, washed with EtOH, water, and MeCN, and dried in air. Yellow crystals of **1d** suitable a single-crystal X-ray analysis were separated manually in the yield of 0.020 g, 7% (based on Fe).

*Syntheses of $[Fe_4Ln_2(O_2CCMe_3)_6(N_3)_4(Htea)_4]\cdot 2(CH_2Cl_2)$ (Ln^{III} = Dy (**2a**); Er (**2b**)).* Recrystallization of **1a** or **1b** from hot dichloromethane yields well-shaped yellow crystals of

DOI: 10.1021/acs.inorgchem.6b02100
Inorg. Chem. 2017, 56, 1814–1822

$[Fe_4Ln_2(O_2CCMe_3)_6(N_3)_4(Htea)_4]\cdot 2(CH_2Cl_2)$ suitable for a single-crystal X-ray diffraction analysis.

2a *{Fe_4Dy_2}*. Elemental analysis calcd. for $C_{56}H_{110}Cl_4Dy_2Fe_4N_{16}O_{24}$ (2081.8 g mol^{-1}): C 32.31, H 5.33, N 10.77%; found: C 32.99, H 5.21, N 10.92%; calcd. mass ratio of Dy/Fe: 1.47; found: 1.52. IR (KBr): ν = 3417 (br, m), 2957 (m), 2900 (m), 2864 (m), 2098 (s), 2076 (vs), 1582 (sh), 1536 (vs), 1482 (s), 1459 (m), 1421 (s), 1402 (s), 1353 (m), 1284 (m), 1226 (m), 1153 (w), 1098 (m), 1068 (m), 1023 (sh), 918 (sh), 901 (m), 788 (w), 740 (w), 651 (m), 623 (sh), 603 (m), 569 (w), 553 (sh), 489 (m), 428 (m) cm^{-1}.

2b *{Fe_4Er_2}*. Elemental analysis calcd. for $C_{56}H_{110}Cl_4Er_2Fe_4N_{16}O_{24}$ (2091.3 g mol^{-1}): C 32.16, H 5.30, N 10.72%; found: C 32.18, H 5.15, N 10.94%; calcd. mass ratio of Er/Fe: 1.50; found: 1.50. IR (KBr): ν = 3422 (br, m), 2957 (m), 2900 (m), 2866 (m), 2098 (s), 2076 (vs), 1582 (sh), 1535 (vs), 1481 (s), 1459 (m), 1421 (s), 1403 (s), 1361 (m), 1284 (m), 1226 (m), 1154 (w), 1099 (m), 1076 (m), 1024 (m), 919 (sh), 902 (m), 788 (w), 741 (w), 655 (m), 626 (m), 602 (m), 569 (m), 555 (sh), 492 (m), 428 (m) cm^{-1}.

*Syntheses of $[Fe_4Ln_2(O_2CCMe_3)_4(N_3)_6(Htea)_4]\cdot 2(CH_2Cl_2)\cdot 2(EtOH)$ (Ln^{III} = Dy (**3a**); Er (**3b**))*. A solution of $[Fe_3O(O_2CCMe_3)_6(EtOH)_3]NO_3\cdot(EtOH)$ (0.208 g, 0.2 mmol), $Ln(NO_3)_3\cdot xH_2O$ (0.3 mmol), NaN_3 (0.058 g, 0.9 mmol), and H_3tea (0.084 g, 0.6 mmol) in 20 mL of a EtOH/CH_2Cl_2 (1:1) mixture was refluxed for 4 h and then filtered. The filtrate was kept at room temperature. After 10 d, yellow crystals of **3a** and **3b** were filtered off, washed with EtOH and ether, and dried in air. Yield (based on Fe): 0.105 g, 34% (**3a**); 0.085 g, 28% (**3b**).

3a *{Fe_4Dy_2}*. Elemental analysis calcd. for $C_{50}H_{104}Cl_4Dy_2Fe_4N_{22}O_{22}$ (2055.8 g mol^{-1}): C 29.21, H 5.10, N 14.99%; found: C 29.37, H 5.01, N 15.70%; calcd. mass ratio of Dy/Fe: 1.45; found: 1.51. IR (KBr): ν = 3421 (br, m), 2960 (m), 2900 (m), 2862 (m), 2097 (s), 2077 (vs), 2051 (s), 1535 (vs), 1483 (s), 1459 (m), 1422 (s), 1365 (m), 1352 (sh), 1285 (m), 1228 (m), 1149 (w), 1094 (m), 1072 (m), 1062 (sh), 1024 (m), 920 (sh), 900 (m), 788 (w), 740 (w), 649 (m), 626 (sh), 608 (m), 552 (m), 489 (m), 428 (m) cm^{-1}.

3b *{Fe_4Er_2}*. Elemental analysis calcd. for $C_{50}H_{104}Cl_4Er_2Fe_4N_{22}O_{22}$ (2065.3 g mol^{-1}): C 29.08, H 5.08, N 14.92; found: C 29.07, H 4.85, N 15.93%; calcd. mass ratio of Er/Fe: 1.50; found: 1.47. IR (KBr): ν = 3422 (br, m), 2961 (m), 2900 (m), 2862 (m), 2098 (s), 2077 (vs), 2051 (s), 1533 (vs), 1483 (s), 1460 (m), 1422 (s), 1365 (m), 1352 (sh), 652 (m), 626 (sh), 602 (m), 555 (m), 493 (m), 428 (m) cm^{-1}.

Syntheses of $[Fe_{18}M_6(O_2CCHMe_2)_{12}(Htea)_{18}(tea)_6(N_3)_6]\cdot n$(solvent), ($M^{III}$ = Dy (4, 4a), Gd (5), Tb (6), Ho (7), Sm (8), Eu (9), and Y (10)). ***4*** *{$Fe_{18}Dy_6$}*. A solution of $[Fe_3O(O_2CCHMe_2)_6(H_2O)_3]NO_3\cdot 2(MeCN)\cdot 2(H_2O)$ (0.082 g, 0.087 mmol), $Dy(NO_3)_3\cdot 6(H_2O)$ (0.064 g, 0.18 mmol), sodium azide (0.02 g, 0.3 mmol), and triethanolamine (0.26 g, 1.74 mmol) in MeOH/MeCN (1:1, 12 mL) was ultrasonicated for 35 min at room temperature and then filtered. The filtrate was allowed to slowly evaporate at room temperature. This resulted in yellow crystals suitable for single-crystal X-ray diffraction of the first polymorph of **4** after one week. The crystals were filtered off, washed with methanol, and dried under vacuum. Crystals of **4**, $[Fe_{18}Dy_6(O_2CCHMe_2)_{12}(Htea)_{18}(tea)_6(N_3)_6]\cdot(MeCN)\cdot 8(H_2O)$, lost their crystallinity upon loss of crystal solvent. Yield: 0.03 g (30% based on Fe). Elemental analysis calcd. for $4\cdot 8(H_2O)$, $C_{192}H_{406}Dy_6Fe_{18}N_{42}O_{104}$, 6947.7 g mol^{-1}): C, 33.19; H, 5.89; N, 8.47; Dy, 14.03; Fe, 14.47%. Found: C, 32.01; H, 5.63; N, 8.08; Dy, 13.7; Fe, 14.3%. IR (KBr): 3423 (br), 2964 (sh), 2862 (s), 2064 (vs), 2036 (sh), 1568 (m), 1472 (m), 1384 (sh), 1359 (m), 1284 (w), 1096 (vs), 898 (m), 750 (w), 1019 (sh), 592 (vw), 559 (vw), 457 (vw) cm^{-1}.

4a *{$Fe_{18}Dy_6$}*. A solution of $[Fe_3O(O_2CCHMe_2)_6(H_2O)_3]NO_3\cdot 2(MeCN)\cdot 2(H_2O)$ (0.082 g, 0.087 mmol) in EtOH (6 mL) was added to a solution of $Dy(NO_3)_3\cdot 6(H_2O)$ (0.031 g, 0.09 mmol), sodium azide (0.02 g, 0.3 mmol), and triethanolamine (0.26 g,1.47 mmol) in MeOH (6 mL). The resulting solution was ultrasonicated for 75 min at room temperature. Following filtration, the filtrate was left for slow evaporation, producing yellow crystals of the second polymorph, **4a**. Yield: 0.028 g (26% based on Fe). Elemental analysis calcd. for **4a** $[Fe_{18}Dy_6(O_2CCHMe_2)_{12}(Htea)_{18}(tea)_6(N_3)_6]\cdot 6(MeOH)\cdot 30(H_2O)$, $C_{198}H_{474}Dy_6Fe_{18}N_{42}O_{132}$, 7536.5 g mol^{-1}: C 31.55, H 6.34, N 7.81; Dy, 12.94; Fe, 13.34%. Found: C 32.47, H 5.90, N 8.28; Dy, 12.9; Fe, 14.5%. IR (KBr): 3423 (br), 2964 (sh), 2864 (s), 2064 (vs), 2036 (sh), 1630 (vw), 1565 (m), 1471 (w), 1415 (w), 1359 (w), 1284 (vw), 1162 (sh), 1096 (vs), 898 (m), 750 (vw), 560 (vw), 469 (vw) cm^{-1}. Compounds **5**–**10** were obtained in an analogous manner to that of **4**.

5 *{$Fe_{18}Gd_6$}*. Yield: 0.02 g (20% based on Fe), $[Fe_{18}Gd_6(O_2CCHMe_2)_{12}(Htea)_{18}(tea)_6(N_3)_6](MeCN)\cdot 10(H_2O)$. Elemental analysis calcd. for $5\cdot 10(H_2O)$, $C_{194}H_{413}Gd_6Fe_{18}N_{43}O_{106}$, 6952.2 g mol^{-1}: C 33.17, H 5.94, N 8.46; Gd, 13.57; Fe, 14.46%. Found: C 33.46, H 5.63, N 8.33; Gd, 13.4; Fe, 12.5%. IR (KBr): 3423 (br), 2962 (s), 2920 (sh), 2854 (m), 2064 (m), 2036 (sh), 1570 (m), 1473 (s), 1471 (w), 1415 (w), 1359 (w), 1281 (w), 1164 (w), 1075 (m), 898 (m), 748 (sh), 560 (vw) cm^{-1}.

6 *{$Fe_{18}Tb_6$}*. Yield: 0.017 g (16% based on Fe), $[Fe_{18}Tb_6(O_2CCHMe_2)_{12}(Htea)_{18}(tea)_6(N_3)_6]\cdot 2(MeCN)\cdot 8(MeOH)\cdot 7.5(H_2O)$. Elemental analysis calcd. for $6\cdot 8(MeOH)\cdot 7.5(H_2O)$, $C_{200}H_{437}Fe_{18}N_{42}O_{111.5}Tb_6$, 7173.6 g mol^{-1}: C, 33.49; H, 6.14; N, 8.20; Tb, 13.29; Fe, 14.01%. Found: C, 33.08; H, 6.00; N, 8.29; Tb, 13.4; Fe, 14.3%. IR (KBr): 3418 (br), 2963 (sh), 2861 (s), 2063 (vs), 2036 (sh), 1569 (m), 1472 (m), 1415 (m), 1358 (m), 1284 (w), 1163 (sh), 1086 (vs), 897 (m), 829 (sh), 749 (vw), 591 (w), 559 (w), 460 (w) cm^{-1}.

7 *{$Fe_{18}Ho_6$}*. Yield: 0.017 g (16% based on Fe). $[Fe_{18}Ho_6(O_2CCHMe_2)_{12}(Htea)_{18}(tea)_6(N_3)_6]\cdot 2(MeCN)\cdot 3(MeOH)\cdot 11.5(H_2O)$. Elemental analysis calcd. for $7\cdot 3(MeOH)\cdot 11.5(H_2O)$, $C_{195}H_{425}Fe_{18}Ho_6N_{42}O_{110.5}$, 7121.5 g mol^{-1}: C, 32.89; H, 6.01; N, 8.26%. Found: C, 33.43; H, 6.03; N, 7.47%. IR (KBr): 3423 (br), 2964 (sh), 2864 (s), 2063 (vs), 2036 (sh), 1571 (m), 1472 (m), 1416 (m), 1359 (w), 1285 (w), 1164 (sh), 1076 (vs), 898 (m), 750 (vw), 593 (vw), 559 (vw), 459 (vw) cm^{-1}.

8 *{$Fe_{18}Sm_6$}*. Yield: 0.017 g (16% based on Fe). $[Fe_{18}Sm_6(O_2CCHMe_2)_{12}(Htea)_{18}(tea)_6(N_3)_6]\cdot 3(MeCN)\cdot 14(MeOH)\cdot 24(H_2O)$. Elemental analysis calcd. for $8\cdot 14(MeOH)\cdot 24(H_2O)$, $C_{206}H_{494}Fe_{18}N_{42}O_{134}Sm_6$, 7611.7 g mol^{-1}: C, 32.50; H, 6.54; N, 7.73%. Found: C, 33.13; H, 5.87; N, 8.31%. IR (KBr): 3426 (br), 2960 (sh), 2920 (sh), 2852 (m), 2064 (m), 2036 (sh), 1629 (w), 1565 (m), 1469 (w), 1414 (m), 1359 (w), 1283 (vw), 1075 (s), 898 (m), 488 (vw) cm^{-1}.

9 *{$Fe_{18}Eu_6$}*. Yield: 0.02 g (20% based on Fe). $[Fe_{18}Eu_6(O_2CCHMe_2)_{12}(Htea)_{18}(tea)_6(N_3)_6]\cdot 2(MeCN)\cdot 5(MeOH)\cdot 8(H_2O)$. Elemental analysis calcd. for $9\cdot 5(MeOH)\cdot 8(H_2O)$, $C_{197}H_{426}Eu_6Fe_{18}N_{42}O_{109}$, 7044.7 g mol^{-1}: C, 33.59; H, 6.03; N, 8.35%. Found: C, 33.73; H, 6.36; N, 8.67%. IR (KBr): 3340 (br), 2962 (sh), 2920 (sh), 2853 (m), 2065 (m), 2036 (sh), 1631 (w), 1568 (m), 1470 (w), 1415 (w), 1359 (w), 1284 (vw), 1076 (s), 898 (m), 560 (vw), 489 (vw) cm^{-1}.

10 *{$Fe_{18}Y_6$}*. Yield: 0.017 g (17% based on Fe). $[Fe_{18}Y_6(O_2CCHMe_2)_{12}(Htea)_{18}(tea)_6(N_3)_6]\cdot 3(MeCN)\cdot 9(MeOH)\cdot 11(H_2O)$. Elemental analysis calcd. for $10\cdot 11(H_2O)$, $C_{198}H_{412}Fe_{18}N_{42}O_{107}Y_6$, 6560.2 g mol^{-1}: C, 35.15; H, 6.33; N, 8.97%. Found: C, 33.68; H, 6.12; N 8.40%. IR (KBr): 3422 (br), 2963 (sh), 2963 (s), 2064 (vs), 2063 (sh), 1544 (m), 1471 (m), 1416 (m), 1359 (m), 1284 (w), 1164 (sh), 1097 (vs), 898 (m), 830 (sh), 750 (vw), 593 (vw), 559 (vw), 462 (vw) cm^{-1}.

Magnetic Measurements. Magnetic susceptibility data of **1**–**10** were recorded using a Quantum Design MPMS-5XL SQUID magnetometer for direct current (dc) and alternating current (ac) measurements. The polycrystalline samples were immobilized into polytetrafluoroethylene capsules. The dc susceptibility data were acquired as a function of the field (0.1–5.0 T) and temperature (2.0–290.0 K). The ac susceptibility data were measured in the absence of a static bias field in the frequency range of 3–1500 Hz (T = 2.0–50.0 K, B_{ac} = 3 G). All data were corrected for diamagnetic contributions from the sample holder and the compounds (as calculated from Pascal's constants; χ_{dia} (1×10^{-3} cm^3 mol^{-1}): **1a**: −1.00, **1b**: −1.01, **1c**: −1.00, **1d**: −0.99, **2a**: −1.05, **2b**: −1.04, **3a**: −1.03, **3b**: −1.03, **4**: −3.46, **5**: −3.45, **6**: −3.45, **7**: −3.47, **8**: −3.43, **9**: −3.43, **10**: −3.24).

X-ray Crystallographic Analyses. Single-crystal X-ray diffraction experiments for **1a**–**c** and **2**–**10** were performed at 100(2) K on a Bruker diffractometer with APEX II CCD detector using graphite-

DOI: 10.1021/acs.inorgchem.6b02100
Inorg. Chem. 2017, 56, 1814–1822

monochromated Mo Kα radiation. Diffraction data sets for **1d** were collected at 100(2) K on an Oxford Xcalibur CCD with graphite-monochromatized Mo Kα radiation. The summary of the data collection and the crystallographic parameters of compounds **1**–**10** are given in Table S1. Full crystallographic data and refinement details of **1**–**10** are provided in Supporting Information. The positions of metal atoms were found by the direct methods. The remaining atoms were located in an alternating series of least-squares cycles and difference Fourier maps. All non-hydrogen atoms were refined in full-matrix anisotropic approximation using the *SHELX* suite of programs.[14] All hydrogen atoms were placed at idealized positions and were allowed to ride on the neighboring atoms. Some hydrogen atoms of solvent molecules: H_2O, MeCN, and MeOH, could not be located in **4**–**10**. In **1a**–**c**, methyl groups for one monodentate pivalate ligand as well as the solvent ethanol molecule were found to be disordered. In **2a** and **2b**, some of the methyl groups in carboxylates and solvate dichloromethane molecule also revealed disorders. In **4**–**10** methyl groups for some isobutyrate ligands, ethanol groups of triethanoamine ligands, as well as azide were found to be also disordered. Therefore, SIMU, DELU, SADI, ISOR, and DFIX restraints were used to deal with the disordered moieties in the structures and to obtain reasonable geometrical parameters and thermal displacement coefficients. Selected bond distances for **1**–**10** are listed in Supporting Information (Table S1), and hydrogen bonding interactions in **1**–**10** are presented in Table S2. Additional crystallographic information and full experimental details can be found in Supporting Information.

RESULTS AND DISCUSSION

The reaction of tri- or hexanuclear pivalate clusters with lanthanide salts, azide, and triethanolamine (H_3tea) ligands in EtOH under reflux leads to wheel-shaped $\{Fe_4Ln_2\}$-type cluster compounds $[Fe_4Ln_2(O_2CCMe_3)_6(N_3)_4(Htea)_4]\cdot 2(EtOH)$ (Ln^{III} = Dy (**1a**), Er (**1b**), and Ho (**1c**)), $[Fe_4Tb_2(O_2CCMe_3)_6(N_3)_4(Htea)_4]$ (**1d**) in 7–43% yield, and the homometallic octanuclear Fe^{III} cluster $[Fe_8O_3(O_2CCMe_3)_6(N_3)_3(tea)(Htea)_3]\cdot 0.5(EtOH)$ in 30% yield. Recrystallization of **1a** and **1b** from hot dichloromethane afforded crystals of $[Fe_4Ln_2(O_2CCMe_3)_6(N_3)_4(Htea)_4]\cdot 2(CH_2Cl_2)$ (Ln^{III} = Dy (**2a**) and Er (**2b**)). Boiling of the same starting materials in mixture of CH_2Cl_2/EtOH (1:1) resulted in the heterometallic wheels $[Fe_4Ln_2(O_2CCMe_3)_4(N_3)_6(Htea)_4]\cdot 2(EtOH)\cdot 2(CH_2Cl_2)$ (Ln^{III} = Dy (**3a**) and Er (**3b**), where two terminal carboxylic groups were replaced by two azide ligands.

By changing the reaction conditions (using MeOH/MeCN or MeOH/EtOH (1:1) mixtures at room temperature) and introducing trinuclear Fe^{III} μ_3-oxo isobutyrate as precursor, we obtained ultralarge $\{Fe_{18}M_6\}$-type wheels, isolated as $[Fe_{18}M_6(O_2CCHMe_2)_{12}(Htea)_{18}(tea)_6(N_3)_6]\cdot n(solvent)$ for M^{III} = Dy (**4**, **4a**), Gd (**5**), Tb (**6**), Ho (**7**), Sm (**8**), Eu (**9**), and Y (**10**), which accumulated in 16–30% yields over one week.

The IR spectra of **1**–**10** display strong bands in the 1565–1533 cm^{-1} and 1417–1406 cm^{-1} regions that arise from the asymmetric and symmetric vibrations of the carboxylate groups from the coordinated pivalates or isobutyrates, respectively. The C–H asymmetric and symmetric stretching vibrations for methyl groups of carboxylates are observed between 2959 and 2870 cm^{-1}, while the asymmetric and symmetric bending vibrations for these groups produce a strong single band at 1483 cm^{-1} and a doublet (1374–1355 cm^{-1}), respectively. The uncoordinated hydroxyl groups of $Htea^{2-}$ and solvent EtOH or H_2O molecules result in broad bands (3420–3375 cm^{-1}). A sharp peak at 2062 cm^{-1} corresponds to the N≡N stretching vibrations of azide ligands in all compounds.

TGA of **1**–**10** showed that all compounds exhibit similar thermal decomposition behavior and release the remaining solvent molecules below 190 °C (Figures S24–S38). When further heated, the wheels start to decompose in several weakly resolved steps until ~800 °C. The decomposition of organic ligands in the smaller $\{Fe_4Ln_2\}$ wheels is accompanied by exothermic peaks at 209 and 222 °C (**1a**), 200 °C (**2a**), 199 °C (**3a**), 212 °C (**1b**), 212 °C (**2b**), 199 °C (**3b**), 189 °C (**1c**), and 187 °C (**2c**).

Structural Description. *$\{Fe_4Ln_2\}$ Wheels.* Single-crystal X-ray diffraction analysis reveals that **1**–**3** comprise wheel-shaped centrosymmetric hexanuclear $[Fe_4Ln_2(O_2CCMe_3)_6(N_3)_4(Htea)_4]$ (**1** and **2**) and $[Fe_4Ln_2(O_2CCMe_3)_4(N_3)_6(Htea)_4]$ (**3**) clusters (see Figure 2) built from four Fe^{III} and two Ln^{III} ions that are linked by an array of bridging carboxylate, azide, and aminopolyalcoholato-based ligands into a cyclic structure with a cavity, and crystal solvent molecules: two EtOH per formula unit in **1a**–**c**, two CH_2Cl_2 in **2**, and two EtOH and two

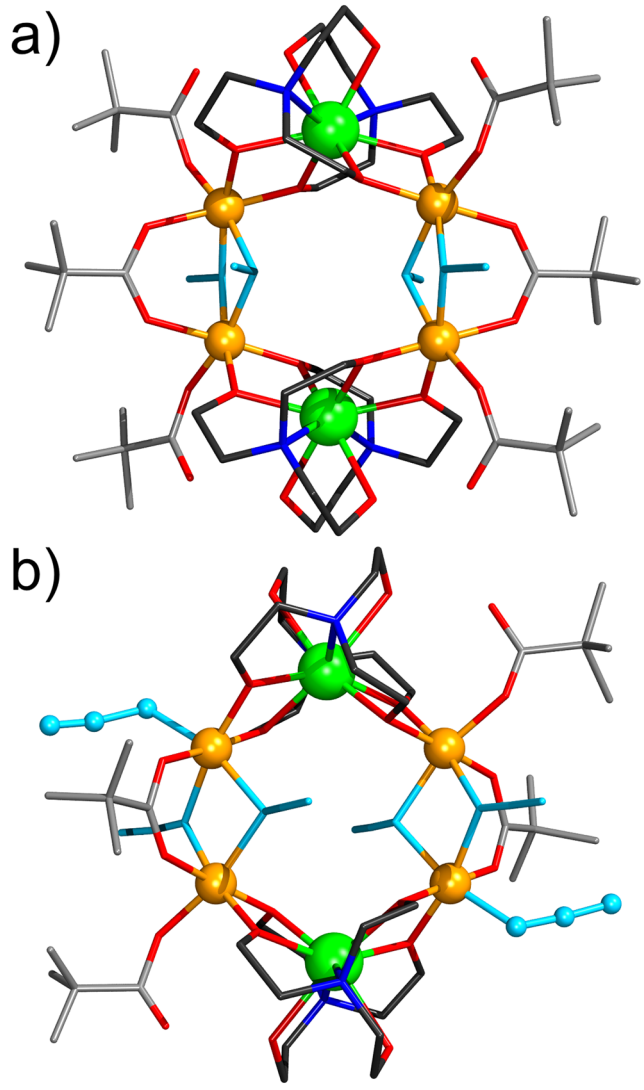

Figure 2. Structures of wheel-shaped $\{Fe_4Ln_2\}$ clusters in **1** and **2** (a) and **3** (b). Color scheme: C(tea), dark gray; C(pivalate), light gray; O, red; N(tea), blue; N(azide), light blue); Ln, green; Fe, dark yellow spheres. Monodentate N_3^- groups in **3** are highlighted as light blue spheres. Hydrogen atoms are omitted for clarity.

DOI: 10.1021/acs.inorgchem.6b02100
Inorg. Chem. 2017, 56, 1814–1822

CH_2Cl_2 in **3**. The asymmetric units of **1** and **2** contain one Ln^{III} and two Fe^{III} centers, two monodentate and one bridging carboxylate groups, two $Htea^{2-}$ and two end-on bridging N_3^- ligands, and one solvent molecule, whereas the asymmetric unit of **3** contains one Ln^{III} and two Fe^{III} ions, one monodentate and one bridging carboxylate groups, two $Htea^{2-}$, one monodentate and two end-on bridging N_3^- ligands, and two solvent molecules.

Each Fe^{III} atom in **1** and **2** resides in a distorted octahedral N_2O_4 environment made from two azide ligands [Fe−N_{azide}, 2.085(6)−2.152(7) Å], two O sites from two carboxylates [Fe−O_{carb}, 1.963(4)−2.071(6) Å], and two alcoholate sites of two $Htea^{2-}$ [Fe−O_{alc}, 1.937(4)−1.982(5) Å]. In **3**, the two independent Fe^{III} centers adopt different environments: one Fe^{III} in a distorted octahedral N_2O_4 environment analogous to **1** and **2** [Fe−N_{azide}, 2.095(10)−2.137(10) Å, Fe−O_{carb}, 1.969(9)−2.053(8) Å, Fe−O_{alc}, 1.925(8)−1.949(12) Å]. The second Fe^{III} adopts a distorted octahedral N_3O_3 geometry arising from three N atoms of three azide ligands [Fe−N_{azide}, 2.036(10)−2.135(13) Å], one carboxylate O atom [Fe−O_{carb}, 2.018(14)−2.031(9) Å], and two alcoholates from two $Htea^{2-}$ [Fe−O_{alc}, 1.933(12)−1.940(8) Å]. The azido-bridged Fe···Fe distances are 3.221(2)−3.279(2) Å, with Fe−N_{azide}−Fe bridging angles of 98.4(2)−101.6(4)° in **1**−**3**.

Each Ln^{III} atom in **1**−**3** is eight-coordinated by donor atoms of two $Htea^{2-}$ molecules: two N [Ln−N, 2.602(5)−2.612(5) (**1a**); 2.586(5)−2.591(5) (**1b**); 2.579(5)−2.581(5) (**1c**); 2.598(5)−2.601(5) (**2a**); 2.603(7)−2.607(7) (**2b**); 2.597(13)−2.598(13) (**3a**); 2.576(9)−2.584(9) (**3b**) Å] and six O sites [Ln−O, 2.283(3)−2.414(3) (**1a**); 2.272(4)−2.389(4) (**1b**); 2.258(4)−2.380(4) (**1c**); 2.284(4)−2.396(4) (**2a**); 2.270(6)−2.397(5) (**2b**); 2.294(12)−2.417(11) (**3a**); 2.278(8)−2.367(8) (**3b**) Å]. Neighboring Fe^{III} polyhedra share a common N−N edge, while Ln^{III}−Fe^{III} polyhedra share O−O edges in **1**−**3**. Nearest-neighbor Fe···Fe distances range from 3.220(2) to 3.279(2) Å, Fe···Ln from 3.361(1) to 3.398(1) Å.

In **1**−**3**, the uncoordinated pivalate C═O group and the OH group in $Htea^{2-}$ as well as the solvate EtOH and CH_2Cl_2 molecules participate in an extensive network of hydrogen bonds with both strong O−H···O and O−H···N interactions, and C−H···O, C−H···N, and C−H···Cl contacts (for more details see Supporting Information and Figures S9−S15); these interactions significantly influence the crystal packing.[15]

In the crystal lattices of **1**−**3**, coplanar wheels are stacked along columns. Interestingly, in **1** and **2** these columns are related by translations *b* and *c* and thus have the same orientation of wheels, while in **3**, the columns of stacked wheels alternate in their orientation with respect to the position of Fe or Ln ions (Figures S16−S19).

{$Fe_{18}M_6$} Wheels. Single-crystal X-ray analyses revealed that compounds **4**, **5**, **6**, **7**, **9**, and **10** crystallize in the triclinic space group $P\bar{1}$ and have C_i symmetry, whereas **4a** and **8** crystallize in the trigonal space group $R\bar{3}$ and have C_{3i} crystallographic symmetry. The molecular core structures in **4**−**10** involve 18 Fe^{III} and 6 Ln^{III}/Y^{III} ions interconnected by six isobutyrate and 24 amino alcohol ligands into a ring with alternating three Fe^{III} and one Ln^{III}/Y^{III} ions. The wheels are slightly puckered with Fe···Fe···Fe angles of ca. 140° and Fe···Ln/Y···Fe angles of ca. 114° and form a central cavity with a diameter of ca. 1 nm, Figure 3, while the external diameter of ultralarge wheels is ca. 3.7 nm. The crystal structures of ultralarge wheels display infinite channels filled by solvent molecules (Figure 3c) parallel to the crystallographic *c* axis for **4a** and **8** and along *a* for the

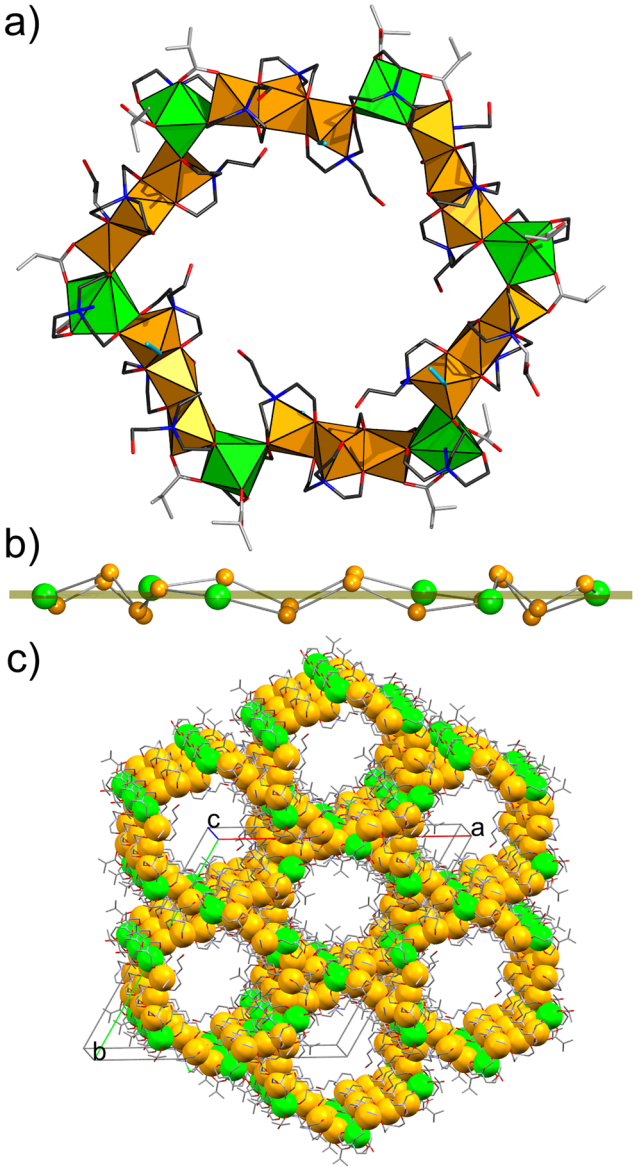

Figure 3. (a) Molecular structure of {$Fe_{18}M_6$} wheels in **4**−**10**. Fe/Ln/Y centers are highlighted as their coordination polyhedra (color code as in Figure 2). Hydrogen and disordered atoms are omitted for clarity. (b) Side view of the {$Fe_{18}M_6$} metal skeleton; the transparent yellow plane serves to emphasize the small deviations from a fully planar ring structures. (c) Formation of infinite channels in the trigonal crystal lattices of **4a** and **8** along *c* (for triclinic structures see Supporting Information).

remaining structures. Upon removal of neutral solvent molecules, the triclinic structures reveal a large total potential solvent area volume of ca. 27%, and trigonal one ca. 44% per unit cell volume, as calculated by PLATON.

All Fe centers in **4**−**10** are in a distorted octahedral ligand environment: 12 Fe atoms have a NO_5 donor set, and the remaining six Fe atoms have a N_2O_4 donor set. The NO_5 environments are formed by a bridging isobutyrate (one O), three amino alcoholate ligands (three O), and a doubly deprotonated $Htea^{2-}$ (one N) or by one tea^{3-} and two doubly deprotonated $Htea^{2-}$ (five O, one N). The N_2O_4 set stems from three amino alcohols (four O), from a doubly deprotonated $Htea^{2-}$ (one N) and one azide N atom. All of the Fe−O bond distances in **4**−**10** are in the range of

DOI: 10.1021/acs.inorgchem.6b02100
Inorg. Chem. 2017, 56, 1814−1822

1.876(12)−2.060(5) Å (Fe−O_{carb}: 2.021(11)−2.060(5), Fe−O_{alc}: 1.876(12)−2.051(11) Å). Fe−N_{azide} distances range from 1.992(1) to 2.064(12) Å, whereas Fe−N_{alc} distances are distinctly longer (2.201(7)−2.327(15) Å). All Ln and Y sites are in distorted square-antiprismatic NO_7 environments (Ln/Y−O: 2.259(6)−2.469(6), Ln/Y−N: 2.602(7)−2.698(16) Å) made from two $Htea^{2-}$ and one tea^{3-} (five O, one N), and O atoms of the bridging and monodentate carboxylates. The latter is additionally linked by a strong intramolecular O−H···O bond. Fe···Fe distances amount to 3.162(3)−3.222(4) Å, Ln/Y···Fe to 3.354(1)−3.534(1) Å. Neighboring coordination polyhedra in **4**−**10** share common O−O edges (Figure 3a).

Magnetic Properties. *{Fe_4Ln_2} Wheels.* Magnetic ac and dc susceptibility data of compounds **1**−**3** were collected using a SQUID magnetometer. The magnetic dc data of **1**−**3** are presented as $\chi_m T$ versus T plots in Figure 4. At 290 K, the $\chi_m T$ data of **1**−**3** reach values in the interval 39−46 cm^3 K mol^{-1}. All values are in the upper half of the ranges that are expected for four Fe^{III} and the two respective Ln^{III} non-interacting, high-spin centers: 44.2 (**1a**), 44.7 (**2a**), 45.8 (**3a**), expected:[16] 42.3−46.1 cm^3 K mol^{-1}. Found: 39.9 (**1b**), 39.8 (**2b**), 39.6 (**3b**), expected: 38.4−40.6; 44.6 (**1c**), expected: 42.8−45.6; 41.1 (**1d**), expected: 39.8−42.0 cm^3 K mol^{-1}. $\chi_m T$ steadily increases with decreasing T, exhibiting a steep slope at $T \leq 50$ K revealing dominant ferromagnetic exchange interactions within the compounds, potentially between all pairs of next neighbors. Note that compounds **3a** and **3b** containing additional azide ligands exhibit maxima at larger $\chi_m T$ values than their analogues, pointing to an effective enhancement of ferromagnetic exchange interactions due to these ligands.

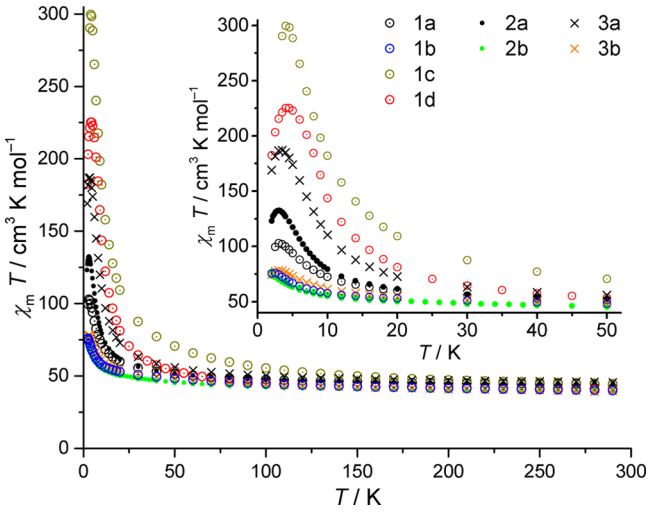

Figure 4. Temperature dependence of $\chi_m T$ at B = 0.1 T of **1**−**3**.

Susceptibility measurements (ac) were performed to probe slow magnetization relaxation of compounds **1**−**3**. At zero static dc field, only **1c** and **1d** showed significant out-of-phase signals down to 2 K and up to 1500 Hz. Out-of-phase signals could be detected up to 3 K for **1c** (see Figure S39). Because of the constraints of the parameter range of our experimental setup, however, the collected data were insufficient for further phenomenological modeling, for example, via an Arrhenius-like expression. For **1d**, out-of-phase signals at zero bias field are present up to 5.5 K (see Figures 5 and S40). A generalized Debye expression[17] is simultaneously fit to the frequency-dependent in-phase χ'_m and out-of-phase χ''_m components of the magnetic ac susceptibility in the range of 2.2 K $\leq T \leq$ 4.2 K. Analysis of the resulting attempt time τ versus T^{-1} data in the 2.6−4.0 K interval in terms of an Arrhenius expression ($\tau = \tau_0 \cdot \exp(U_{eff}/(k_B \cdot T))$) yields parameters typically observed[7,18] for Orbach relaxation processes: $\tau_0 = (1.2 \pm 0.2) \times 10^{-9}$ s and $U_{eff} = (26.4 \pm 0.4)$ cm^{-1}.

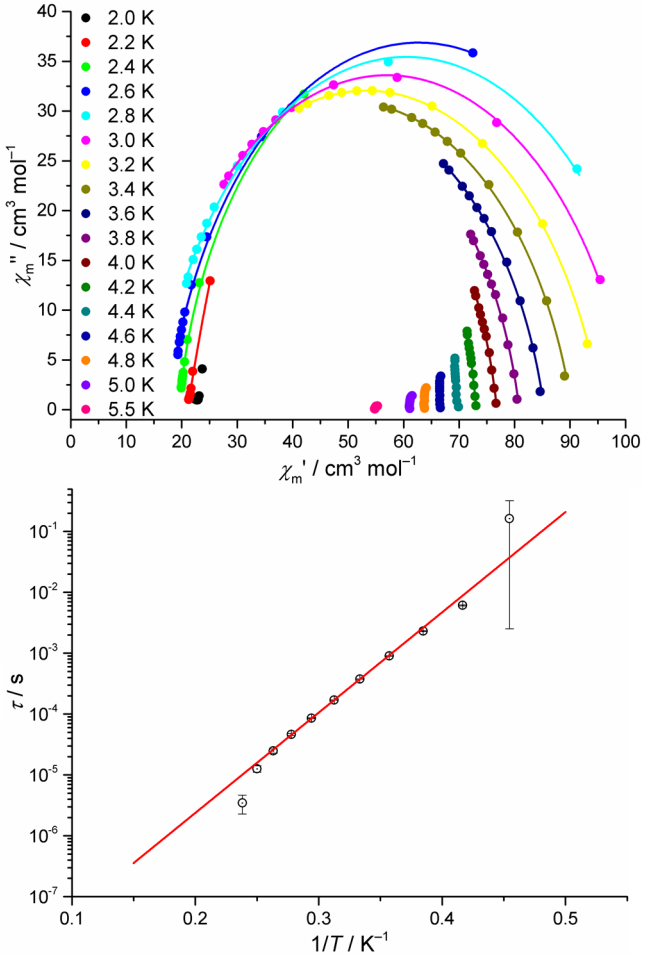

Figure 5. (top) Cole−Cole plot of in-phase χ'_m and out-of-phase χ''_m susceptibility of **1d** at various temperatures and zero static bias field: experimental data (●), least-squares fits (solid lines). (bottom) Corresponding Arrhenius plot of relaxation time τ vs T^{-1} (2.2 K $\leq T \leq$ 4.2 K), solid line shows fit to an Orbach relaxation expression (2.6 K $\leq T \leq$ 4.0 K).

{$Fe_{18}M_6$} Wheels. The magnetic properties of **4**−**10** were investigated by both dc and ac measurements. Analysis of **10** (comprising diamagnetic yttrium centers instead of lanthanides) reveals the magnetism of the Fe^{III} constituents. In a first approximation, these form six linear Fe_3 trimers, separated by the Y^{III} centers. Assuming a symmetric cluster and normalizing the data to such a linear trimer results in the magnetic properties shown in Figure 6 as open circles.

The $\chi_m T$ value of 7.99 cm^3 mol^{-1} at 290 K (B = 0.1 T) is well below the range of 12.19−13.51 cm^3 mol^{-1} that is expected for three non-interacting Fe^{III} centers.[16] By lowering the temperature, $\chi_m T$ continuously decreases to 3.59 cm^3 mol^{-1} at 14 K and, below that point, more rapidly to 2.36 cm^3 mol^{-1} at 2 K. The molar magnetization M_m versus B at 2 K is likely to saturate in the range of 5−7 $N_A \mu_B$ revealing an upper limit of the total spin of the ground state, which is below 15/2, the maximum spin value for three ferromagnetically coupled spin-

DOI: 10.1021/acs.inorgchem.6b02100
Inorg. Chem. 2017, 56, 1814−1822

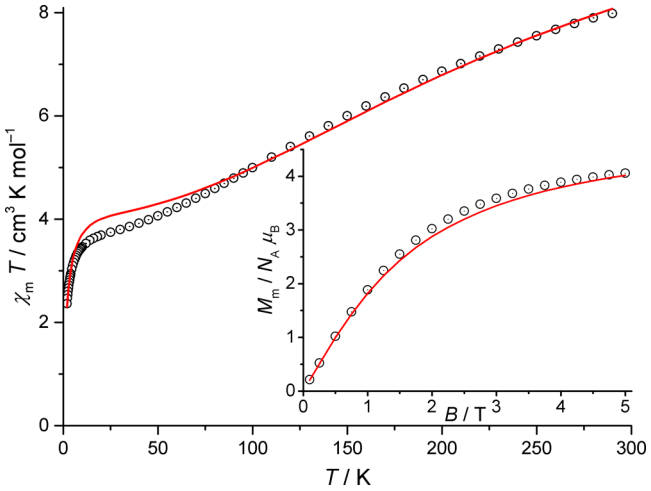

Figure 6. Magnetic properties of **10**, normalized to a Fe^{III}_3 unit: Temperature dependence of $\chi_m T$ at B = 0.1 T (○: experimental data, straight lines: calculated data (S_{eff} = 5/2 spin system)); inset: molar magnetization M_m vs applied field B at T = 2.0 K.

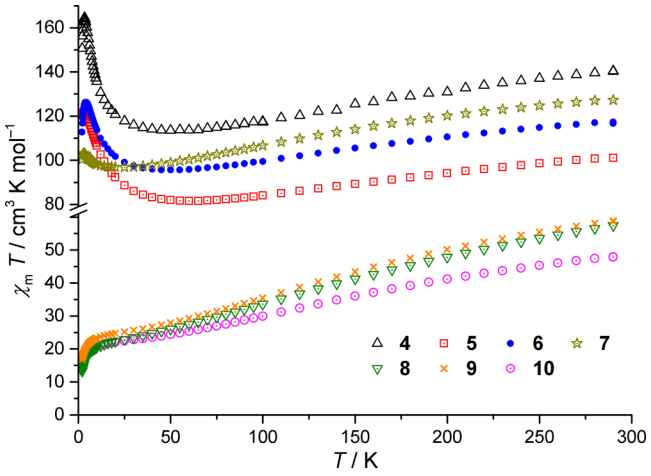

Figure 7. Temperature dependence of $\chi_m T$ at B = 0.1 T of **4**–**10**.

like Fe^{III} centers. All three observations combined indicate predominant anti-ferromagnetic exchange interactions within each Fe_3 unit.

The magnetic data can thus be modeled as six weakly coupled, identical linear trimers of three spin-5/2 centers for slightly distorted octahedrally coordinated Fe^{III} centers using the computational framework CONDON 2.0.[19] Potential interactions between neighboring Fe_3 groups are accounted for by an (isotropic) molecular field approach. The best fit (SQ = 4.1%) reproduces the experimental data as shown in Figure 6, yielding J_{Fe3} = −12.4 cm^{-1} ($H_{ex} = -2J_{Fe3}$ ($S_1 \cdot S_2 + S_2 \cdot S_3$), g = 2.0) for both intratrimer exchange interaction energies and λ_{mf} = −0.412 mol cm^{-3}, that is, zJ_{inter} = −0.21 cm^{-1}. According to the fit, the magnitude and sign of J_{Fe3} thus reveal anti-ferromagnetic exchange interactions within an Fe_3 group characterized by a ground state of $S_{eff,total}$ = 5/2. Additionally, such a trimer and the molecular field are linked by weak anti-ferromagnetic interactions. Note that the obvious deviation of experiment and fit in the 5–90 K interval is presumably due to a slightly more complex exchange interaction scheme than the employed model and, to a much lesser or even negligible extent, caused by ligand-field effects linked to the distortion of the octahedral site symmetry of the Fe^{III} centers. Nevertheless, the main contributions of the exchange interactions are reasonably described by the presented model.

The magnetic data of **10** are compared to the data for **4**–**9** in Figure 7. The $\chi_m T$ values at 290 K of the compounds are ca. 25–30 cm^3 K mol^{-1} below the expected values[19] for the respective non-interacting centers of a $\{Fe_{18}Ln_6\}$ ring (**4**: 140.5 cm^3 K mol^{-1}, **5**: 101.2 cm^3 K mol^{-1}, **6**: 117.3 cm^3 K mol^{-1}, **7**: 127.2 cm^3 K mol^{-1}, **8**: 57.4 cm^3 K mol^{-1}, **9**: 58.9 cm^3 K mol^{-1}, **10**: 47.9 cm^3 K mol^{-1}). It is reasonable to infer an almost constant high-temperature $\chi_m T$ offset for all compounds, including **10**, that primarily arises from the anti-ferromagnetic interactions within the linear Fe^{III}_3 trimers discussed above. Additionally, the $\chi_m T$ curves of **4**, **5**, **6**, and **7** also show ferromagnetic interactions within the ring structure revealed by the distinct maxima at ∼3–4 K. In case of **8** and **9**, no maxima are observed, which is due to the almost temperature-independent paramagnetism (TIP)-like behavior of the Sm^{III} centers (**8**, multiplets characterized by energetically very close states) and Eu^{III} centers (**9**, m_J = 0 ground state), respectively.[16] The ferromagnetic exchange interactions are most likely between the terminal Fe^{III} centers of the linear trimers and the next-neighbor Ln^{III} centers, since the corresponding signal is only observed in the presence of the centers that are not characterized by temperature-independent contributions. The similar decrease in $\chi_m T$ upon cooling the compounds from 290 K to ca. 100 K is thus potentially only caused by anti-ferromagnetic coupling interactions between the Fe^{III} centers of the trimer units.

The molar magnetization measured at different applied fields B and at 2.0 K (see Figure S41) is consistent with the conclusions derived from the $\chi_m T$ data: the magnetizations of all compounds approximately add up to the magnetization of **10** and up to 6 times the maximum contribution of the respective Ln ($g_J J$ $N_A \mu_B$). Note that M_m of **10** hints at a saturation value that is much lower than the maximum possible value of 90 $N_A \mu_B$ for 18 Fe^{III} centers indicating the anti-ferromagnetic interactions within a ring. For **4**, **5**, **6**, and **7**, the deviations from the maximum Ln contributions may be due to anisotropic Fe–Ln exchange interactions, due to different magnitudes of the exchange coupling energies or due to single ion contributions of the Ln^{III} centers, that is, the ground state of the Ln^{III} centers may be characterized by $m_J \neq \pm J$ and thus by a less-than-maximum magnetic moment.

In addition to the dc measurements, **4**–**10** were measured in an ac magnetic field in absence of a static field. Only **4** and **6** show any out-of-phase signal and thus slow relaxation above 2.0 K and below 1500 Hz (see Figures S42 and S43, respectively). Because of the limits of our experimental setup, only small temperature intervals with $\chi''_m \neq 0$ and no distinct features like maxima in χ''_m are observed; thus, the ac data are insufficient for further analysis of relaxation characteristics. We thus can only conclude that slow relaxation occurs for **4** at $T \leq$ 2.3 K and for **6** at $T \leq$ 2.6 K.

CONCLUSION

In summary, a synthetic strategy exploiting the potential of structure-directed semiflexible bridging ligands and solvent effects has been successfully applied to design and prepare a new family of hexanuclear $\{Fe_4Ln_2\}$ wheels as well as the currently largest d/f coordination wheels, the tetraicosanuclear $\{Fe_{18}Ln_6\}$ clusters. $\{Fe_4Tb_2\}$ (**1d**), $\{Fe_4Ho_2\}$ (**1c**), $\{Fe_{18}Dy_6\}$

DOI: 10.1021/acs.inorgchem.6b02100
Inorg. Chem. 2017, 56, 1814–1822

(**4**), and {$Fe_{18}Tb_6$} (**6**) were found to exhibit slow magnetization relaxation.

■ ASSOCIATED CONTENT

Supporting Information

The Supporting Information is available free of charge on the ACS Publications website at DOI: 10.1021/acs.inorgchem.6b02100.

Crystallographic data (cif files of **1**−**10**); scheme of the syntheses; details of structural determination; table of selected bond distances; table of hydrogen bonding interactions; the asymmetric unit in **1**−**3** with a numbering scheme; a view of hydrogen bonds in **1**−**3**; packing diagrams for **1**−**10**; TGA/DTA curves; additional magnetic ac and dc susceptibility data. (PDF)

Crystallographic data (CIF)
Crystallographic data (CIF)
Crystallographic data (CIF)
Crystallographic data (CIF)
Crystallographic data (CIF)
Crystallographic data (CIF)
Crystallographic data (CIF)
Crystallographic data (CIF)
Crystallographic data (CIF)
Crystallographic data (CIF)
Crystallographic data (CIF)
Crystallographic data (CIF)
Crystallographic data (CIF)
Crystallographic data (CIF)
Crystallographic data (CIF)
Crystallographic data (CIF)
Crystallographic data (CIF)

■ AUTHOR INFORMATION

Corresponding Authors

*E-mail: paul.koegerler@ac.rwth-aachen.de. Phone: +49-241-80-93642. Fax: +39-241-80-92642. (P.K.)

*E-mail: sbaca_md@yahoo.com. Phone: +373-22-738154. Fax: +373-22-738149. (S.G.B.)

ORCID

Paul Kögerler: 0000-0001-7831-3953

Svetlana G. Baca: 0000-0002-2121-2091

Author Contributions

The manuscript was written through contributions of all authors.

Notes

The authors declare no competing financial interest.

CCDC 927262 (**1a**); 927263 (**1b**); 927264 (**1c**); 1500364 (**1d**); 927265 (**2a**); 927266 (**2b**); 927267 (**3a**); 927268 (**3b**); 1500366 (**4**); 1500369 (**4a**); 1500368 (**5**); 1500365 (**6**); 1500367 (**7**); 1500370 (**8**); 1500371 (**9**); and 1500372 (**10**) contain the supplementary crystallographic data for this paper. These data can be obtained free of charge from the Cambridge Crystallographic Data Centre via www.ccdc.cam.ac.uk/data_request/cif.

■ ACKNOWLEDGMENTS

This work was supported by the EU (POLYMAG, IIF Contract No. 252984; ERC Starting Grant No. 308051, MOLSPINTRON) and the State Program of the Republic of Moldova (Project No. 16.00353.50.05A). Authors thank U. Englert for collecting X-ray diffraction data sets for **1a**−**c** and **2**−**10** and N. Izarova for collecting the dataset for **1d**. O.B. acknowledges a DAAD fellowship.

■ REFERENCES

(1) (a) McInnes, E. J. L.; Timco, G. A.; Whitehead, G. F. S.; Winpenny, R. E. P. Heterometallic Rings: Their Physics and Use as Supramolecular Building Blocks. *Angew. Chem., Int. Ed.* **2015**, *54*, 14244−14269. (b) Schmidt, H.-J.; Schröder, C.; Luban, M. Modulated spin waves and robust quasi-solitons in classical Heisenberg rings. *J. Phys.: Condens. Matter* **2011**, *23*, 386003.

(2) (a) Taft, K. L.; Delfs, C. D.; Papaefthymiou, G. C.; Foner, S.; Gatteschi, D.; Lippard, S. J. $[Fe(OMe)_2(O_2CCH_2Cl)]_{10}$, a Molecular Ferric Wheel. *J. Am. Chem. Soc.* **1994**, *116*, 823−832. (b) King, P.; Stamatatos, T. C.; Abboud, K. A.; Christou, G. Reversible Size Modification of Iron and Gallium Molecular Wheels: A Ga_{10} "Gallic Wheel" and Large Ga_{18} and Fe_{18} Wheels. *Angew. Chem., Int. Ed.* **2006**, *45*, 7379−7383.

(3) (a) Murugesu, M.; Raftery, J.; Wernsdorfer, W.; Christou, G.; Brechin, E. K. Synthesis, Structure, and Magnetic Properties of a $[Mn_{22}]$ Wheel-like Single-Molecule Magnet. *Inorg. Chem.* **2004**, *43*, 4203−4209. (b) Tasiopoulos, A. J.; Vinslava, A.; Wernsdorfer, W.; Abboud, K. A.; Christou, G. Giant Single-Molecule Magnets: A $\{Mn_{84}\}$ Torus and Its Supramolecular Nanotubes. *Angew. Chem., Int. Ed.* **2004**, *43*, 2117−2121.

(4) Cadiou, C.; Murrie, M.; Paulsen, C.; Villar, V.; Wernsdorfer, W.; Winpenny, R. E. P. Studies of a nickel-based single molecule magnet: resonant quantum tunnelling in an S = 12 molecule. *Chem. Commun.* **2001**, 2666−2667.

(5) (a) Gerbeleu, V.; Struchkov, Yu. T.; Timko, G. A.; Batsanov, A. S.; Indrichan, K. M.; Popovich, G. A. *Dokl. Akad. Nauk SSSR* **1990**, *313*, 1459−1462. (b) van Slageren, J.; Sessoli, R.; Gatteschi, D.; Smith, A. A.; Helliwell, M.; Winpenny, R. E. P.; Cornia, A.; Barra, A.-L.; Jansen, A. G. M.; Rentschler, E.; Timco, G. A. Magnetic Anisotropy of the Antiferromagnetic Ring $[Cr_8F_8Piv_{16}]$. *Chem. - Eur. J.* **2002**, *8*, 277−285.

(6) (a) Affronte, M.; Carretta, S.; Timco, G. A.; Winpenny, R. E. P. A ring cycle: studies of heterometallic wheels. *Chem. Commun.* **2007**, 1789−1797. (b) Timco, G. A.; McInnes, E. J. L.; Winpenny, R. E. P. Physical studies of heterometallic rings: an ideal system for studying magnetically-coupled systems. *Chem. Soc. Rev.* **2013**, *42*, 1796−806. (c) Fernandez, A.; Ferrando-Soria, J.; Pineda, E. M.; Tuna, F.; Vitorica-Yrezabal, I. J.; Knappke, C.; Ujma, J.; Muryn, C. A.; Timco, G. A.; Barran, P. E.; Ardavan, A.; Winpenny, R. E. P. Making hybrid [n]-rotaxanes as supramolecular arrays of molecular electron spin qubits. *Nat. Commun.* **2016**, *7*, 10240. (d) Ferrando-Soria, J.; Moreno Pineda, E.; Chiesa, A.; Fernandez, A.; Magee, S. A.; Carretta, S.; Santini, P.; Vitorica-Yrezabal, I. J.; Tuna, F.; Timco, G. A.; McInnes, E. J. L.; Winpenny, R. E. P. A modular design of molecular qubits to implement universal quantum gates. *Nat. Commun.* **2016**, *7*, 11377.

(7) Woodruff, D. N.; Winpenny, R. E. P.; Layfield, R. A. Lanthanide Single-Molecule Magnets. *Chem. Rev.* **2013**, *113*, 5110−5148.

(8) Langley, S. K.; Moubaraki, B.; Forsyth, C. M.; Gass, I. A.; Murray, K. S. Structure and magnetism of new lanthanide 6-wheel compounds utilizing triethanolamine as a stabilizing ligand. *Dalton Trans.* **2010**, *39*, 1705−1708.

(9) (a) Li, M.; Ako, A. M.; Lan, Y.; Wernsdorfer, W.; Buth, G.; Anson, C. E.; Powell, A. K.; Wang, Z.; Gao, S. New heterometallic $[Mn^{III}_4Ln^{III}_4]$ wheels incorporating formate ligands. *Dalton Trans.* **2010**, *39*, 3375−3377. (b) McRobbie, A.; Sarwar, A. R.; Yeninas, S.; Nowell, H.; Baker, M. L.; Allan, D.; Luban, M.; Muryn, C. A.; Pritchard, R. G.; Prozorov, R.; Timco, G. A.; Tuna, F.; Whitehead, G. F. S.; Winpenny, R. E. P. Chromium chains as polydentate fluoride ligands for lanthanides. *Chem. Commun.* **2011**, *47*, 6251−6253. (c) Zou, L.-F.; Zhao, L.; Guo, Y.-N.; Yu, G.-M.; Guo, Y.; Tang, J.; Li, Y.-H. A dodecanuclear heterometallic dysprosium−cobalt wheel exhibiting single-molecule magnet behavior. *Chem. Commun.* **2011**, *47*, 8659−8661.

(10) (a) Schray, D.; Abbas, G.; Lan, Y.; Mereacre, V.; Sundt, A.; Dreiser, J.; Waldmann, O.; Kostakis, G. E.; Anson, C. E.; Powell, A. K.

DOI: 10.1021/acs.inorgchem.6b02100
Inorg. Chem. 2017, 56, 1814−1822

Combined Magnetic Susceptibility Measurements and ^{57}Fe Mössbauer Spectroscopy on a Ferromagnetic {$Fe^{III}_4Dy_4$} Ring. *Angew. Chem., Int. Ed.* **2010**, *49*, 5185−5188. (b) Schmidt, S.; Prodius, D.; Novitchi, G.; Mereacre, V.; Kostakis, G. E.; Powell, A. K. Ferromagnetic heteronuclear {$Fe_4(Er,Lu)_2$} cyclic coordination clusters based on ferric wheels. *Chem. Commun.* **2012**, *48*, 9825−9827.

(11) (a) Foguet-Albiol, D.; Abboud, K. A.; Christou, G. High-nuclearity homometallic iron and nickel clusters: Fe_{22} and Ni_{24} complexes from the use of *N*-methyldiethanolamine. *Chem. Commun.* **2005**, 4282−4284. (b) Rinck, J.; Novitchi, G.; Van den Heuvel, W.; Ungur, L.; Lan, Y.; Wernsdorfer, W.; Anson, C. E.; Chibotaru, L. F.; Powell, A. K. An Octanuclear [$Cr^{III}_4Dy^{III}_4$] 3d−4f Single-Molecule Magnet. *Angew. Chem., Int. Ed.* **2010**, *49*, 7583−7587. (c) Li, M.; Lan, Y.; Ako, A. M.; Wernsdorfer, W.; Anson, C. E.; Buth, G.; Powell, A. K.; Wang, Z.; Gao, S. A Family of 3d-4f Octa-Nuclear [$Mn^{III}_4Ln^{III}_4$] Wheels (Ln = Sm, Gd, Tb, Dy, Ho, Er, and Y): Synthesis, Structure, and Magnetism. *Inorg. Chem.* **2010**, *49*, 11587−11594. (d) Baniodeh, A.; Hewitt, I. J.; Mereacre, V.; Lan, Y.; Novitchi, G.; Anson, C. E.; Powell, A. K. Heterometallic 20-membered {$Fe_{16}Ln_4$} (Ln = Sm, Eu, Gd, Tb, Dy, Ho) metallo-ring aggregates. *Dalton. Trans.* **2011**, *40*, 4080−4086.

(12) (a) Baca, S. G.; van Leusen, J.; Speldrich, M.; Kögerler, P. Understanding the magnetism of {Fe_2Ln} dimers, step-by-step. *Inorg. Chem. Front.* **2016**, *3*, 1071−1075. (b) Malaestean, I. L.; Ellern, A.; Baca, S.; Kögerler, P. Cerium oxide nanoclusters: commensurate with concepts of polyoxometalate chemistry? *Chem. Commun.* **2012**, *48*, 1499−1501. (c) Malaestean, I. L.; Speldrich, M.; Ellern, A.; Baca, S. G.; Kögerler, P. Heterometal expansion of oxozirconium carboxylate clusters. *Dalton Trans.* **2011**, *40*, 331−333.

(13) (a) Botezat, O.; van Leusen, J.; Ch. Kravtsov, V.; Ellern, A.; Kögerler, P.; Baca, S. G. Iron(III) carboxylate/aminoalcohol coordination clusters with propeller-shaped Fe_8 cores: approaching reasonable exchange energies. *Dalton Trans.* **2015**, *44*, 20753−20762. (b) Baca, S. G.; Speldrich, M.; van Leusen, J.; Ellern, A.; Kögerler, P. Undecametallic and hexadecametallic ferric oxo−hydroxo/ethoxo pivalate clusters. *Dalton Trans.* **2015**, *44*, 7777−7780. (c) Baca, S. G.; Breukers, S.; Ellern, A.; Kögerler, P. An octanuclear iron(III) isobutyrate wheel. *Acta Crystallogr., Sect. C: Cryst. Struct. Commun.* **2011**, *C67*, m371−m374. (d) Baca, S. G.; Speldrich, M.; Ellern, A.; Kögerler, P. {Fe_6O_2}-Based Assembly of a Tetradecanuclear Iron Nanocluster. *Materials* **2011**, *4*, 300−310.

(14) Sheldrick, M. A short history of SHELX. *Acta Crystallogr., Sect. A: Found. Crystallogr.* **2008**, *A64*, 112−122.

(15) (a) Desiraju, G. R.; Steiner, T. *The Weak Hydrogen Bond in Structural Chemistry and Biology;* Oxford University Press: Oxford, 1999. (b) Steiner, T. The hydrogen bond in the solid state. *Angew. Chem., Int. Ed.* **2002**, *41*, 48−76. (c) Desiraju, G. R. A Bond by Any Other Name. *Angew. Chem., Int. Ed.* **2011**, *50*, 52−59. (d) Desiraju, G. R. Reflections on the Hydrogen Bond in Crystal Engineering. *Cryst. Growth Des.* **2011**, *11*, 896−898.

(16) Lueken, H. *Magnetochemie;* Teubner: Stuttgart, Germany, 1999.

(17) Cole, K. S.; Cole, R. H. Dispersion and Absorption in Dielectrics I. Alternating Current Characteristics. *J. Chem. Phys.* **1941**, *9*, 341−351.

(18) Rosado Piquer, L.; Sanudo, E. C. Heterometallic 3d−4f single-molecule magnets. *Dalton Trans.* **2015**, *44*, 8771−8780.

(19) (a) van Leusen, J.; Speldrich, M.; Schilder, H.; Kögerler, P. Comprehensive Insight into Molecular Magnetism via CONDON: Full vs. Effective Models. *Coord. Chem. Rev.* **2015**, *289−290*, 137−148. (b) Speldrich, M.; Schilder, H.; Lueken, H.; Kögerler, P. A Computational Framework for Magnetic Polyoxometalates and Molecular Spin Structures: CONDON 2.0. *Isr. J. Chem.* **2011**, *51*, 215−227.

DOI: 10.1021/acs.inorgchem.6b02100
Inorg. Chem. 2017, 56, 1814−1822